NUMERICAL EVALUATION OF THE STATIC PERFORMANCE OF A SMALL PROPELLER COMPARING TRADITIONAL AND TRANSITIONAL TURBULENCE MODELS

AVALIAÇÃO NUMÉRICA DO DESEMPENHO ESTÁTICO DE UMA PEQUENA HÉLICE COMPARANDO MODELOS DE TURBULÊNCIA TRADICIONAIS E TRANSICIONAIS

EVALUACIÓN NUMÉRICA DEL DESEMPEÑO ESTÁTICO DE UNA HÉLICE PEQUEÑA COMPARANDO MODELOS DE TURBULENCIA TRADICIONALES Y TRANSICIONALES

https://doi.org/10.56238/sevened2026.008-190

Luiz Carlos Bevilaqua dos Santos Reis[1], Newton Galvão de Campos Leite[2], Maurício Araujo Zanardi[3], Laura Manuci de Andrade[4], Rodrigo Viana de Freitas Santos[5]

ABSTRACT

Propeller design and performance influence the operational efficiency of drones, and with the increasing use of small UAVs, accurately determining the performance of small propellers becomes crucial. CFD is considered a highly accurate method, and turbulence models are essential for CFD simulations, especially when dealing with low Reynolds number flows, such as those in small propellers, since transitional laminar-turbulent flows are difficult to predict. The objective of this work is to investigate the use of transition- sensitive models to identify the conditions under which their use is truly necessary, as they are computationally intensive. A 3D-printed propeller, designed from the SDA 1075 airfoil, was tested under static flow conditions on a test bench, with thrust and torque measurements. Fully turbulent models were used in the simulation, and the results were compared with measurements between 2,000 and 8,000 rpm. Consistent results were obtained for Reynolds numbers above 60,000. For Reynolds numbers below 60,000, the results were not very accurate. Therefore, transition-sensitive models capable of capturing laminar separation were used, and consistent results were obtained for Reynolds numbers below 60,000. This was demonstrated by the propeller's aerodynamic coefficients and the images of laminar separation bubbles captured by the simulation.

Keywords: Small-Scale Propellers. CFD. Laminar-Turbulent Transition Models. Experimental Study.

[1] Dr. in Mechanical Engineering. Universidade do Estado do Rio de Janeiro (UERJ). Rio de Janeiro, Brazil. E-mail: bevilaqua@fat.uerj.br
[2] Dr. in Mechanical Engineering. Universidade do Estado do Rio de Janeiro (UERJ). Rio de Janeiro, Brazil. E-mail: nleite@fat.uerj.br
[3] Dr. in Mechanical Engineering. Universidade do Estado do Rio de Janeiro (UERJ). Rio de Janeiro, Brazil. E-mail: mauricio_zanardi@uol.com.br
[4] Graduated in Mechanical Engineering. Universidade do Estado do Rio de Janeiro (UERJ). Rio de Janeiro, Brazil. E-mail: lauramanuci@gmail.com
[5] Undergraduate Student in Mechanical Engineering. Universidade do Estado do Rio de Janeiro (UERJ). Rio de Janeiro, Brazil. E-mail: rodrigo.santos@discentes.fat.uerj.br

RESUMO
O projeto e o desempenho das hélices influenciam a eficiência operacional dos drones e, com o uso crescente de pequenos UAVs, determinar com precisão o desempenho de pequenas hélices torna-se crucial. O CFD é considerado um método altamente preciso, e modelos de turbulência são essenciais para simulações de CFD, especialmente quando se lida com escoamentos de baixo número de Reynolds, como aqueles em pequenas hélices, uma vez que escoamentos laminar-turbulentos transicionais são difíceis de prever. O objetivo deste trabalho é investigar o uso de modelos sensíveis à transição para identificar as condições sob as quais seu uso é realmente necessário, pois são computacionalmente intensivos. Uma hélice impressa em 3D, projetada a partir do aerofólio SDA 1075, foi testada sob condições de fluxo estático em uma bancada de testes, com medições de empuxo e torque. Modelos totalmente turbulentos foram usados na simulação, e os resultados foram comparados com medições entre 2000 e 8000 rpm. Resultados consistentes foram obtidos para números de Reynolds acima de 60.000. Para números de Reynolds abaixo de 60.000, os resultados não foram muito precisos. Portanto, foram utilizados modelos sensíveis à transição capazes de capturar a separação laminar, e resultados consistentes foram obtidos para números de Reynolds abaixo de 60.000. Isso foi demonstrado pelos coeficientes aerodinâmicos da hélice e pelas imagens da separação laminar capturadas pela simulação.

Palavras-chave: Hélices de Pequena Escala. CFD. Modelos de Transição Laminar-Turbulenta. Estudo Experimental.

RESUMEN
El diseño y desarrollo de hélices influyen en la eficiencia operativa de los drones, y con el creciente uso de UAV pequeños, determinar con precisión su rendimiento se vuelve crucial. La CFD se considera un método de alta precisión, y los modelos de turbulencia son esenciales para las simulaciones CFD, especialmente cuando se trabaja con flujos de bajo número de Reynolds, como el de las hélices pequeñas, ya que los flujos laminares-turbulentos transitorios son difíciles de predecir. El objetivo de este trabajo es investigar el uso de modelos sensibles a la transición para identificar las condiciones en las que su uso es realmente necesario, dado su alto consumo computacional. Una hélice impresa en 3D, diseñada con base en el perfil aerodinámico SDA 1075, se probó en condiciones de flujo estático en un banco de pruebas, con mediciones de empuje y par. Se utilizaron modelos completamente turbulentos en la simulación, y los resultados se compararon con mediciones entre 2000 y 8000 rpm. Se obtuvieron resultados consistentes para números de Reynolds superiores a 60.000. Para números de Reynolds inferiores a 60.000, los resultados no son muy precisos. Por lo tanto, se utilizaron modelos sensibles a la transición capaces de capturar la separación laminar, obteniéndose resultados consistentes para números de Reynolds inferiores a 60.000. Esto se demostró mediante los coeficientes aerodinámicos de la hélice e las imágenes de separación laminar capturadas por la simulatión.

Palabras clave: Hélices de Pequeña Escala. CFD. Modelos de Transición Laminar-Turbulenta. Estudio Experimental.

1 INTRODUCTION

In recent years, small unmanned vehicles (UAVs) have been developed for various applications in different areas of our society, being a challenging technology, as designing propellers on a small scale with high efficiency is complex due to the physical phenomena involved. Rotors (engine-propeller assembly) are responsible for the performance and control of fixed-wing and multi-rotor UAVs. They generate thrust and torque that allow drones to fly and remain stable. Propeller design influences the efficiency and stability of drone operation. However, predicting the performance of small-scale propellers, such as those used in UAVs and micro aerial vehicles (MAVs), is complex primarily due to the low Reynolds number conditions under which they operate. Low Reynolds numbers, typically less than 100,000 for UAV propellers (Deters, 2013), can lead to flow separation, which occurs when the fluid boundary layer separates from the blade surface, increasing torque and reducing thrust. This phenomenon occurs when the boundary layer confronts an opposing pressure gradient.

Among the propeller performance prediction techniques, the most accurate is CFD (Loureiro, 2021). The SST k-ω turbulence model is the most widely used in simulations to model propellers. It was developed to improve accuracy in conditions of flow separation and rotating flows. Although laminar-turbulent transition models are recommended for transitional flows and low Reynolds numbers since they take into account the transition region, there are few recently published CFD works that have used laminar-turbulent transition models for propellers. Due to the very fine mesh required near the blade to accurately resolve the transition region, especially for leading and trailing edges, these transitional turbulence models are computationally intensive. And some authors (Loureiro, 2021, and Seeni, 2021) concluded that the SST k-ω model and the laminar-turbulent transition models have similar accuracy, except for flows under static conditions, as mentioned by Loureiro, who observed a significant difference in this condition. Divazi et al., 2025, performed numerical and experimental modeling to study the impact of the distance between the propeller and the atomizer on the spraying performance of agricultural UAVs. The SST k-ω turbulence model and a multiple reference frame technique were used for flow field and particle tracking. The propeller used was a 1045 DJI. They concluded that there is a correlation between the distance between the propeller and the atomizer and the spraying efficiency, and that the study provided important insights into drone spraying systems. Dougherty S. et al., 2024, examined the impact of a 10 × 5.0 propeller separation on quadcopter performance through numerical modeling. They employed the SST k-ω turbulence model along with an unstructured tetrahedral mesh that included inflation layers on the propeller surface. Two configurations were considered: a double propeller configuration and a quadcopter, with initial

flow perpendicular and parallel to each configuration. They described the influence on propeller performance. Liu Y. et al., 2024, developed a numerical model to evaluate the ceiling effect in small-scale inclined propellers (APC propellers 10 x 3.3 and 11 x 4.7). The results were validated by comparison with experimental data in a test bench designed for the study. They used a polyhedral mesh with inflation around the blades and the SST k-ω turbulence model. They developed a model to estimate thrust based on the rotor's distance from the ceiling and its angle relative to the ceiling. Liu X. et al., 2023, investigated a small-scale propeller (APC 1045) to analyze its aerodynamic performance through experiments, numerical simulation, and BEMT (Blade Element Momentum Theory) model. They compared the aerodynamic parameters at various free stream speeds to compare the three different methods. The SST k-ω turbulence model was used with tetrahedral mesh with inflation around the blade face. They concluded that BEMT is reliable enough to estimate the aerodynamic parameters. Rajendran P. et al., 2023, analyzed a twin-blade drone propeller (17 in diameter) using numerical modeling. They used the SST k-ω turbulence model with tetrahedral mesh to develop a propeller with improved torque and coefficient of performance, as well as reduced drag. They concluded that numerical validation was able to provide several modifications to the propeller design. Garofano-Soldado et al., 2022, developed a numerical and experimental study of the ground effect on the aerodynamics of small inclined propellers (13 x 4.4) with low Reynolds number. It was demonstrated that the proximity to the ground of inclined propellers decreases the thrust increment due to the ground effect as the angle increases. They proposed a numerical model to show the dependence of thrust on the distance to the ground and the tilt angle. They used the multiple reference method and the SST k-ω turbulence model with tetrahedral mesh. Zarri A. et al., 2022, developed a numerical modeling of a small drone using the SST k-ω turbulence and a polyhedral mesh with inflation on the blade face. The model was coupled with a computational aero acoustic approach. They concluded that the dominant sound sources are due to the interactions of the blades with the other propellers (9.4 in diameter) and struts, and that the acoustic scattering by the drone has an important effect on the near and far fields. Kumar R. et al., 2021, performed numerical simulation on a quadcopter with 17 x 6.0 propellers operating under different weather conditions. The objective was to predict the effects on services such as photography, remote sensing, aerial surveillance, etc. The standard k-ε turbulence model was employed in combination with a tetrahedral mesh. The modeling was validated against a reference work. Loureiro E. V. et al., 2021, analyzed the performance of small propellers (14 x 7.0) through experiments and using blade element theory in comparison with CFD. For the numerical model, they used the SST k-ω turbulence model and the Transition SST model to investigate

the results in the laminar-turbulent transition boundary layer. For low advanced ratio velocities, the blade element theory presented the best results, while for higher advanced ratio velocities, CFD presented the best results. Paz C., et al., 2021, performed a 3D numerical simulation of the operation of a quadcopter drone (9.4 in diameter) using multiple reference frames and sliding meshes with hexahedral cells. They evaluated the application of these methods to an isolated propeller and to a quadcopter, including the effect of ground proximity. The realizable k-ε turbulence model was used. Seeni A., 2021, applied numerical modeling to select the turbulence model for a small drone propeller (APC 10 x 7.0) operating at low Reynolds number. Validated data were obtained for several turbulence models by comparing them with experimental results. He concluded that the standard k-ω model is preferable for future propeller simulations as it has the advantage of being computationally economical without compromising accuracy. The results showed that the SST k-ω and the Transition SST models produce the same accuracy but at a higher cost. Cerny M. et al., 2020, analyzed small propellers (18 in diameter) insulated and ducted to investigate the influence of inlet angles between zero and 180 degrees with respect to the axial flow. The experimental results showed good agreement with the numerical model, which was developed using a hexahedral mesh and the SST k-ω turbulence model. Deters R. W. et al., 2014, investigated the influence of Reynolds number on the performance of small propellers with diameters between 2.25 and 9 inches. They stated that the low Reynolds number of these propellers makes it very difficult to evaluate their performance. Data from several small propellers under static and continuous flow conditions were measured to study the influence of Reynolds number. The performance improved with increasing Reynolds number, but the maximum efficiency achieved was low compared to larger propellers. They described that at low Reynolds number, a laminar separation bubble forms on the airfoil, and then the laminar boundary layer separates from the surface, becomes turbulent, and may then reattach.

Weerasinghe S.R. et al., 2012, analyzed hovering and flight of the Syma X5SC quadcopter (5.3 in diameter) using CFD and experiments, focusing on the aerodynamic forces on the fuselage and rotor blades. The flight was simulated for hovering mode at three different angles of attack and free-stream velocities. The SST k-ω turbulence model was used with a tetrahedral mesh. They concluded that the simulations adequately described the flows with rotational motions.

This work aims to contribute with a comparative study between experimental results of thrust and torque measurements of a small scale propeller and computational fluid dynamics (CFD) simulation, using the Fluent software. The RANS (Reynols-Averaged Navier-Stokes) turbulence models considered in the simulation were Shear-Stress-Transport

(SST) k-ω, Standard k-ω, Spalart Allmaras and Realizable k-ε. Laminar-turbulent transition models, such as the Transition SST model and the Intermittency Transition model (γ model), were also used to verify the results at low rotations rate, such as 2,000 to 4,000 rpm. In principle, these latter models provide a more realistic simulation of flows where laminar, transitional and turbulent regions coexist, since traditional turbulence models, such as k-ω and k-ε, assume fully developed turbulence, which can lead to incorrect thrust and torque predictions in low Reynolds number flows.

2 EXPERIMENTAL APPARATUS - THRUST, TORQUE AND RPM MEASURING EQUIPMENT

Propeller static performance was conducted on a test rig that was designed to measure propeller thrust, torque and RPM, as shown in Figure 1 and 2. The black propeller is the commercial APC 10 x 4.5 and the white one is an in-house 3D printed propeller. The direct thrust measurement equipment consists of an A2212/6T brushless DC motor (22 mm motor diameter, 12 mm motor shaft height, and 6 turns per pole) used for radio-controlled quadcopters, associated with an electronic speed controller (ESC), a load cell with signal conditioning module HX711 and an infrared obstacle sensor LM393. All devices are interconnected to an Arduino Mega 2560 platform, responsible for synchronized data acquisition.

Figure 1

Test equipment for measuring thrust, torque and RPM

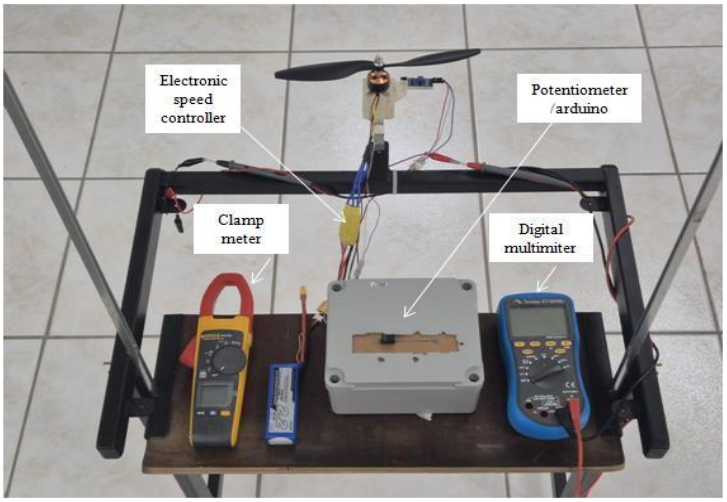

Source: From author.

Figure 2

Front view of the propeller: Fig. 2a; Top view of the propeller: Fig. 2b; Side view of the propeller and RPM measurement sensor: Fig. 2c

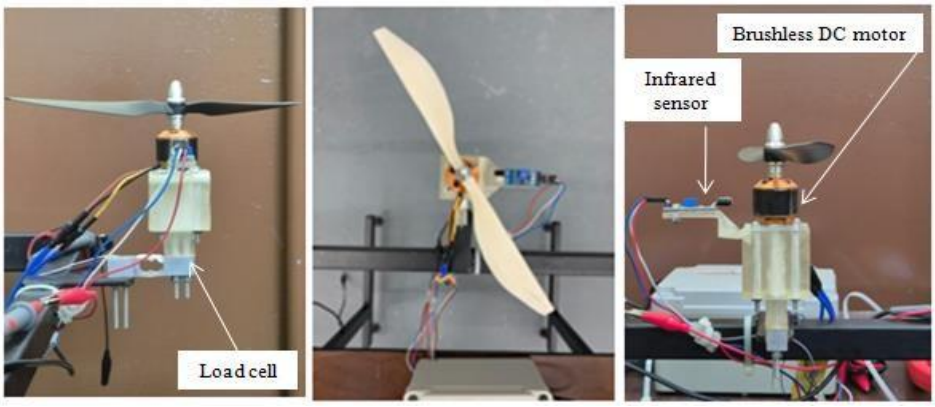

Source: From author.

For indirect torque measurement, a Minipa ET2076-A digital multimeter was used to measure electrical voltage and a Fluke 374 FC clamp meter for non-invasive measurement of electrical current. Electrical power (V x I), multiplied by the motor efficiency, results in mechanical power, which in turn, divided by the angular velocity, is torque. To measure the thrust, a load cell integrated into the HX711 module was used. This sensor converts the mechanical deformation caused by the thrust force generated by the propeller into an electrical signal that can be read by the Arduino platform. The load cell was configured with a variable calibration, which translates the electrical signal from the sensor into mass. The measurement results were then compared with a set of measured masses. The sensor reading is performed in the main loop, which activates the weight sensor, which has a function taking 5 consecutive sensor readings and calculating the average. This procedure reduces the effects of instantaneous variations, improving accuracy. The calibration of the thrust measurement system consisted of three steps: scale factor adjustment, offset compensation via tare, and data acquisition with statistical processing. To determine the scale factor, a set of calibrated masses (2g, 5 g, 10 g, 25 g, 50 g, 100 g, 250 g, 500 g, and 1,000 g) were sequentially applied to the load cell. This procedure verifies the linearity of the sensor over different load ranges. After a 2-second delay for stabilization, the system starts the main loop, where another function performs five consecutive readings and calculates the arithmetic mean, reducing instantaneous variations. The use of varied masses (2 g to 1,000 g) verified the sensitivity of the system at low loads and its ability to maintain accuracy at higher loads, with a post- calibration relative error below 1%.

Propeller rotation was measured using the LM393 reflective sensor, which counts pulses and the time elapsed between them. The sensor emits infrared light onto a rotating

object with alternating reflective and non-reflective segments. The light is reflected from the reflective area and absorbed by the non-reflective area. The phototransistor detects the level of reflection, and the LM393 emits digital pulses. The data acquisition system was programmed using the Arduino IDE platform, integrating the infrared (IR) sensor for rotation measurement with the Arduino Mega 2560 microcontroller. The infrared sensor was positioned at a fixed distance of 1 cm from the brushless motor, with precise alignment to capture rotation signals. During testing, the equipment was turned on and measurements were taken at discrete intervals of 1,000 rpm, covering a range from 2,000 rpm to 8,000 rpm, as recorded by the infrared sensor. Simultaneously, the engine rotation was monitored using the calibrated digital tachometer DT-2234C+, positioned according to the manufacturer's specifications. Before running the test, the propeller was firmly attached to the brushless motor shaft, ensuring mechanical alignment and balancing to avoid parasitic vibrations. The Minipa ET2076-A multimeter, set to measure voltage, and the Fluke 374 FC clamp meter, set to measure direct current, were then connected to the battery terminals to enable simultaneous monitoring of the electrical parameters. The Arduino Mega 2560 was connected to the computer's USB port, with the Serial Monitor open for real-time viewing of the rotation speed, via infrared sensor, and of the force, via load cell. Once the system was set up, the potentiometer was gradually adjusted to increase the motor speed until it reached the predefined maximum of 8,000 rpm.

3 GEOMETRY, GRID GENERATION AND BOUNDARY CONDITIONS

A 10 x 4.5 in house propeller (diameter and pitch, respectively) of two blades was designed, 3D printed, and static tested. The off-the-shelf APC 10 x 4.5 propeller was used to validate the thrust and torque measurements of the developed test rig. The “Design Modeler” software was used to design the propeller, following the characterization methodology proposed by Drella (2006). The process consisted of subdividing the propeller into 10 sections, obtaining the β angle (local geometric blade pitch angle) through a specific formula and scaling the coordinates to the unit chord by dividing the airfoil chord number by 12 mm, corresponding to the chord value in the first airfoil of each blade, as indicated in Table 1, resulting in the propeller geometry. The propeller geometry was created using the SDA1075 airfoil along the entire length of the blades.

Table 1

Data for the geometric dimensions of the propeller

$\beta = arctg\left(\frac{p}{2\pi r}\right)$						
r(mm)	r/R	r (")	chord (")	chord (mm)	β (deg)	scale
19.1	0.15	0.75	0.472	12.0	44	1.000
25.4	0.25	1.00	0.551	14.0	36	1.169
38.1	0.35	1.50	0.819	20.8	26	1.736
50.8	0.45	2.00	0.984	25.0	20	2.087
63.5	0.55	2.50	1.063	27.0	16	2.254
76.2	0.65	3.00	1.055	26.8	13	2.237
88.9	0.75	3.50	1.024	26.0	12	2.170
101.6	0.85	4.00	0.906	23.0	10	1.920
114.3	0.95	4.50	0.709	18.0	9	1.503
127.0	1.00	5.00	0.315	8.0	8	0.668

Source: From author.

The CFD domain for investigating the aerodynamic effects of propeller operation consisted of a wind tunnel with a length of 2.0 m and a width of 1.0 m, and a rotating disk with a radius of 0.137 m and a thickness of 0.03 m around the propeller. The disk was designed to simulate the flow around the propeller. It is a moving reference part that allows modeling a moving component, such as the propeller, by creating this moving frame in a selected cell zone around the propeller. The equations of motion are modified to include the additional terms due to the change from a stationary frame to a moving frame. The propeller becomes a stationary part (Ansys Fluent, 2025). The geometry and mesh of these parts are shown in Figures 3 and 4, respectively. The boundary conditions applied in the simulation are presented in figure 4. As the objective of the analysis is related to the static performance of the propeller (without freestream velocity), both the inlet and outlet airflows were considered as the outlet pressure boundary condition. The axial velocity induced by the rotor at the inlet of the domain is determined by the simulation, with the inlet and outlet boundary conditions being defined by the propeller rotation. In this simulation, the induced inlet flow occurs in the negative direction.

Figure 3

Geometry of wind tunnel and rotating disk

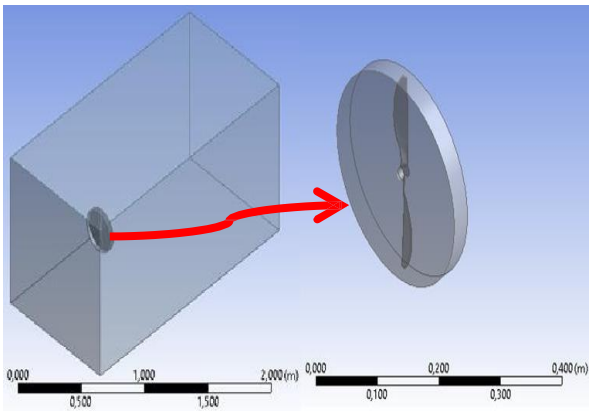

Source: From author.

Figure 4

Mesh and boundary conditions

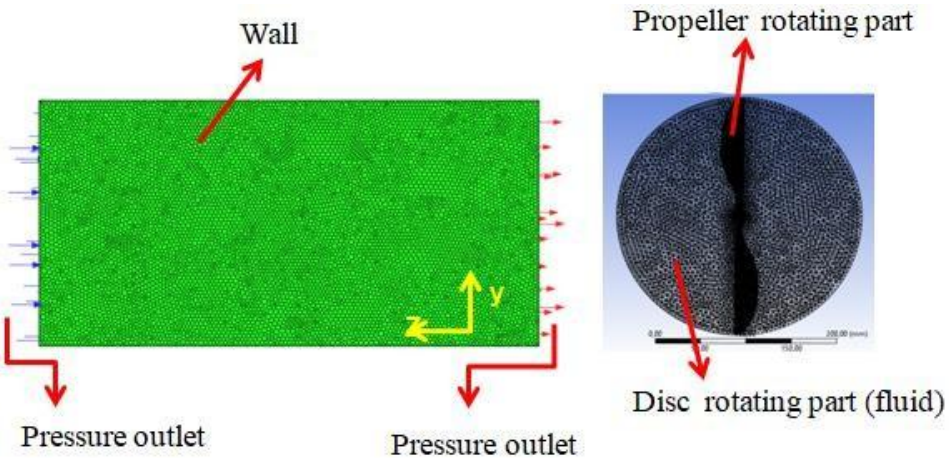

Source: From author.

The chord (c) and twist distribution of the propeller are shown in Fig. 5 and Fig. 6, respectively. As this work was the first project carried out, the profile law constant was chosen (propeller shape constant) and subsequently the thickness (t) distribution is constant, as shown in Fig. 6. Fig. 7 presents how the Reynolds number along the propeller blade varies with different rotational rates.

Figure 5

Chord (c) distribution of designed propeller 10 x 4.5

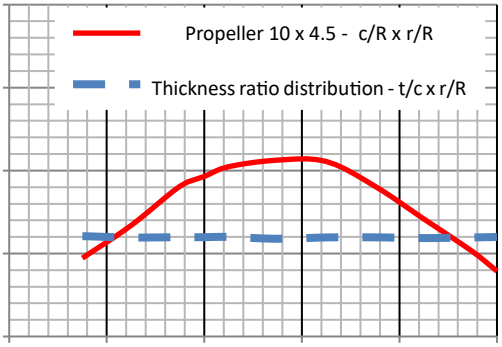

Source: From author.

Figure 6

Twist distribution of designed propeller 10 x 4.5

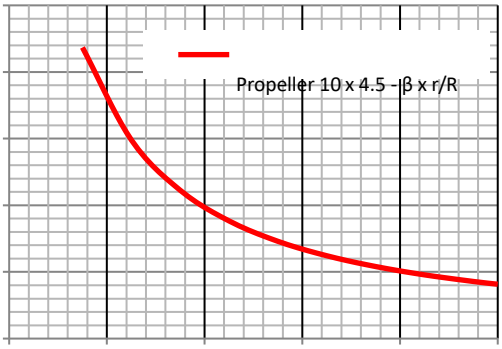

Source: From author.

Figure 7

Reynolds number along the propeller blade

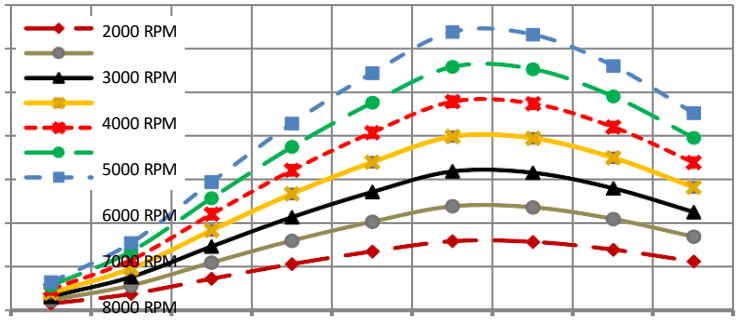

Source: From author.

4 EXPERIMENT PROCEDURES AND VALIDATION

To verify the consistency of the thrust and torque measurement system of the designed propeller, the static performance results of the APC 10 × 4.5 propeller provided by the manufacturer APC Model Aircraft Propellers were used for comparison with the results of measurements performed on this propeller on our test bench. The results are shown in Fig. 8 and Fig. 9.

Figure 8

Thrust coefficient x RPM

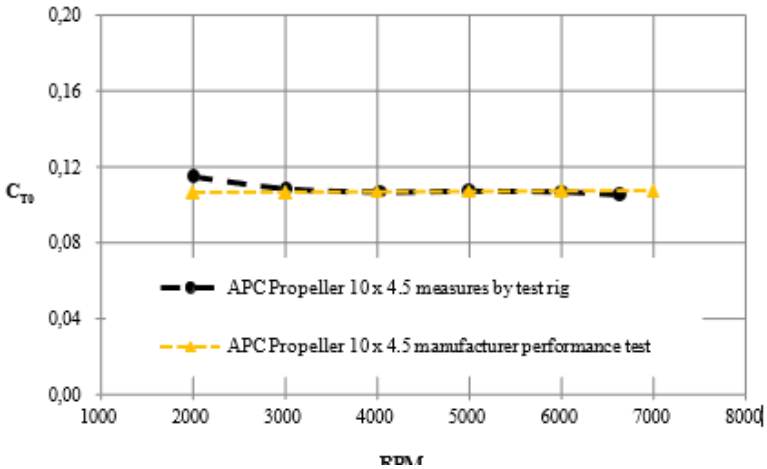

Source: From author.

Figure 9

Power coefficient x RPM

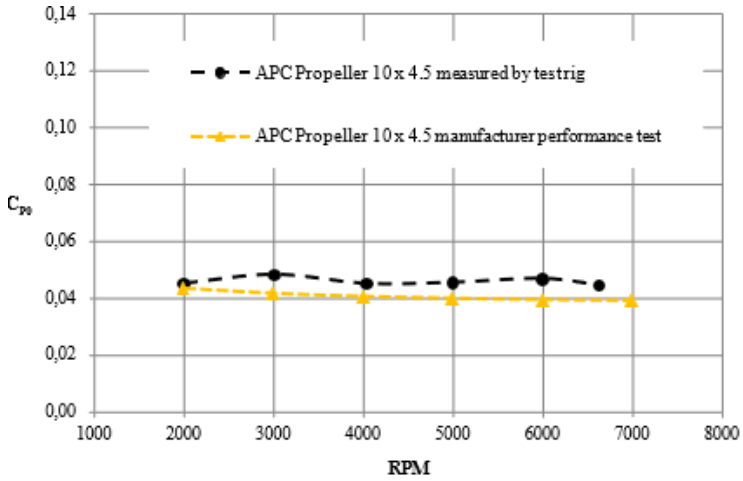

Source: From author.

The thrust coefficient of the APC 10 x 4.5 propeller (Fig. 7) measured by the test equipment in static performance, agrees very well with the manufacturer's performance test, having at 2,000 RPM the greatest difference. The average difference was 2.0% and the maximum was 7.2% at 2,000 RPM.

The power coefficient of the APC 10 × 4.5 propeller (Fig. 8), as measured by the test equipment, differs from the manufacturer's performance data by an average of 11.0%, with a maximum deviation of 15.7% observed at 6,000 RPM. It can be concluded that the test equipment demonstrated satisfactory measurement accuracy and provided a reliable level of confidence for the objectives of this study, which focused on evaluating the most appropriate turbulence model.

5 NUMERICAL MODELS

5.1 RANS EQUATIONS

Four RANS turbulence models were chosen for the numerical simulations. The realizable k-ε model considers the effects of rotations in the definition of the turbulent viscosity, and has already been tested in a single moving reference, as is the case in this modeling, presenting good results. The k-ε models are not recommended when the flow separates under adverse pressure gradients, which is the problem with low Reynolds number propellers (Fluent Theory Guide, 2025). However, as Paz, 2021, used this model in his work and obtained a good result, it will be used to evaluate the current case. The k-ω model provides good results for flows with adverse pressure gradients and airfoils. Low Reynolds numbers can be used with the SST k-ω, and it is a very simple model for laminar-turbulent transition and can be used to predict more accurate details of the wall boundary layer than the Spallart-Allmaras model. SST k-ω is the model most used in recent works with small-scale propellers. The Spallart-Allmaras gives good results for low Reynolds numbers and is designed for boundary layers subject to adverse pressure gradients (Ansys Fluent Theory Guide, 2025).

Partial differential equations (RANS - Reynolds-averaged and Navier-Stokes) are discretized and computed to account for turbulent fluctuations, resulting in Reynolds stresses that must be modeled using a turbulence model. They are typically written in Cartesian coordinates as the following equations, conservation of mass (equation1) and momentum (equation 2), respectively:

$$\frac{\partial \rho}{\partial t} + \frac{\partial}{\partial x_i}(\rho u_i) = 0 \quad (1)$$

$$\frac{\partial}{\partial t}(\rho u_i) + \frac{\partial}{\partial x_j}(\rho u_i u_j) = -\frac{\partial p}{\partial x_i} + \frac{\partial}{\partial x_j}\left[\mu\left(\frac{\partial u_i}{\partial x_j} + \frac{\partial u_j}{\partial x_i} - \frac{2}{3}\delta_{ij}\frac{\partial u_l}{\partial x_l}\right)\right] + \frac{\partial}{\partial x_j}\left(-\rho\overline{u_i' u_j'}\right) \quad (2)$$

Where $-\rho\overline{u_i' u_j'}$ is the Reynolds stress tensor modeled via turbulence models.

Laminar-turbulent transition models augment the RANS equations with extra transport equations or empirical correlations to account for transition phenomena, the change from laminar to turbulent flow, i.e. to predict where and how turbulence begins, which is critical in low Reynolds number flows. The Transition SST model solves two additional equations and is the most used model in the last decade. The Transition γ model (Intermittency Transition

model) solves one additional transport equation and has gained acceptance recently (Ansys Fluent Theory Guide, 2025).

5.2 PROPELLERS COEFFICIENTS

Thrust coefficient: $C_T = \frac{T}{\rho n^2 D^4}$; Power coefficient: $C_P = \frac{P}{\rho n^3 D^5}$; Power: $P = 2\pi n Q$; and Reynold number calculated at velocity of the fluid and chord width at 75% of blade station: $Re = \frac{\rho v_{75} c_{75}}{\mu}$; where $v = \omega r$ for propeller static performance. Where *T* is the propeller thrust; *ρ* is density in kg/m³; *n* is the rotational velocity in revolutions per second; *D* is the diameter of the propeller in m; *Q* is the propeller torque in N.m; and ω is rotational speed in rad/s.

6 GRID INDEPENDENCE ANALYSES

For the fully turbulent models, three 3D tetrahedral meshes with different numbers of cells/nodes were generated to perform independent mesh analyses. Table 2 provides a summary of the sizes of the three meshes. Table 3 shows the mesh quality of this model, using the fine mesh, in comparison to the modeling of a complete quadcopter done by Weerasinghe S.R. et al., 2012, who did a detailed investigation of the mesh quality. This comparison was made between the rotor and the propeller, as well as, between the complete quadcopter and the entire domain of this model. The values demonstrate that the produced mesh is adequate.

Table 2

Mesh size for three different dimensions – tetrahedral

	Coarse mesh	Medium mesh	Fine mesh
Cells	276,531	1,842,868	2,246,122
Faces	802,513	3,958,894	4,783,476
Nodes	108,760	446,658	520,960

Source: From author.

Table 3

Mesh quality analysis – tetrahedra

Mesh quality	Orthogonal (>0.01)		Skewness (<0.95)	
	Minimum	Average	Maximum	Average
Rotor [Weerasinghe, 2012]	0.036	0.82	0.96	0.25
Propeller (current work)	0.222	0.95	0.78	0.59
Full quadcopter [Weerasinghe, 2012]	0.016	0.84	0.96	0.25
Full domain (current work)	0.062	0.75	0.92	0.24

Source: From author.

Figure 10 shows the results of the mesh independence study for the propeller thrust coefficient. The results demonstrate that the fine mesh and the medium mesh present very similar thrust coefficients (average difference of 4%), while the coarser mesh deviates from the other meshes. The SST k-ω model was used to calculate the three different mesh sizes.

Figure 10

Propeller thrust coefficient for comparison of three tetrahedral meshes with different number of cells

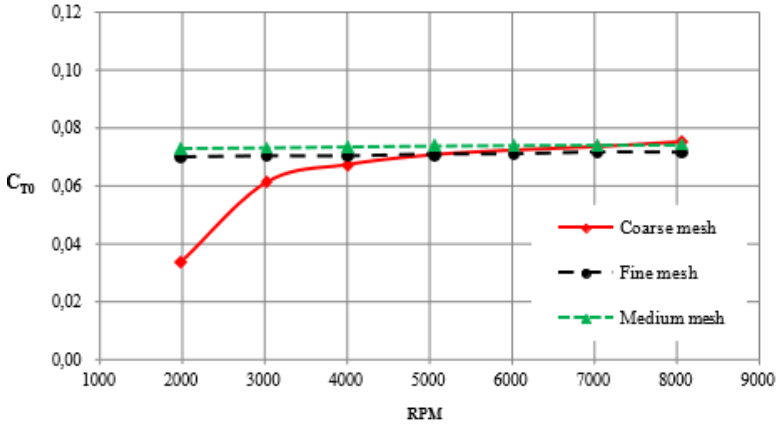

Source: From author.

For analysis with the laminar-turbulent transition models, the mesh was changed to a polyhedral mesh with inflation around the blades. Figure 11 shows the mesh around a propeller airfoil at position r/R = 0.40 (r = 50.8 mm) for two meshes of different sizes. Table 4 shows details of the two polyhedral meshes. Both meshes produced the same results for torque and thrust calculations in the numerical simulation. There was no significant difference.

Table 4

Mesh details for two different sizes – polyhedral with prisms

	Coarse mesh	Fine mesh
Cells	1,707,890	2,808,693
Faces	8,276,454	13,681,975
Nodes	5,505,550	9,128,376
Propeller element size (mm)	1.0	0.8
Disk element size (mm)	2.8	2.0
Transition rate of inflation	0.272	0.272
Layers of inflation	15	20
Growth rate of inflation	1.05	1.02

Source: From author.

Figure 11

Polyhedral mesh with inflation of prisms on the face of the blade: (a) coarse mesh; (b) fine mesh

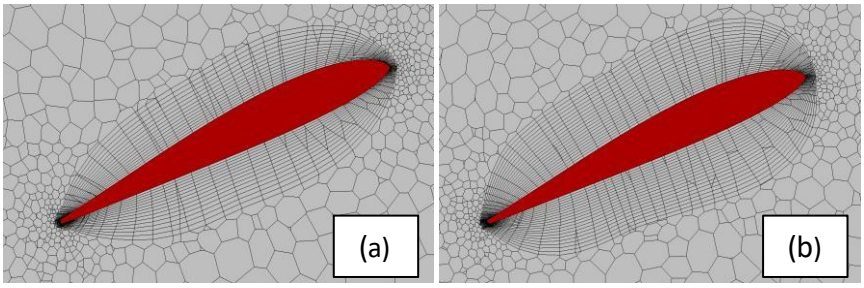

Source: From author.

7 RESULTS AND DISCUSSION

Regarding CFD simulation compared to measurements, the best result was using the SST k-ω turbulence model, as shown in Figs. 12 to 15. With respect the thrust coefficient, the results agreed very well with higher rotation rates and become worse for lower rotation rates (Fig. 12). One explanation for this behavior is related to the lower Reynolds numbers. As shown in Fig. 6, for rotations below 5,000 RPM, Reynolds numbers are less than 60,000 for most of the propeller. This is a typical feature of small-scale propellers and makes performance prediction through CFD less accurate, as the performance of these propellers typically changes with Reynolds numbers. The average difference in thrust coefficients for the SST k-ω model, which obtained the best result, in relation to the measured values, was 5.1% and the maximum difference was 7.6% at 2,000 RPM.

Figure 12

Comparison between CFD-simulated thrust coefficients for various turbulence models with thrust measured on the test bench

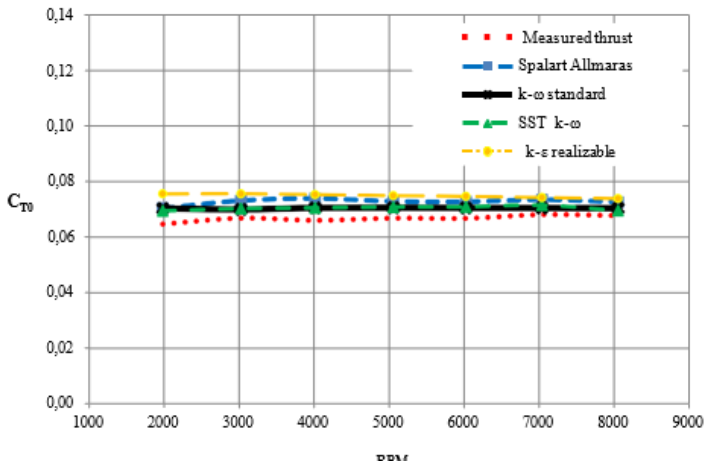

Source: From author.

Figure 13

Comparison between thrust measured on the test bench and simulated by CFD with different turbulence models

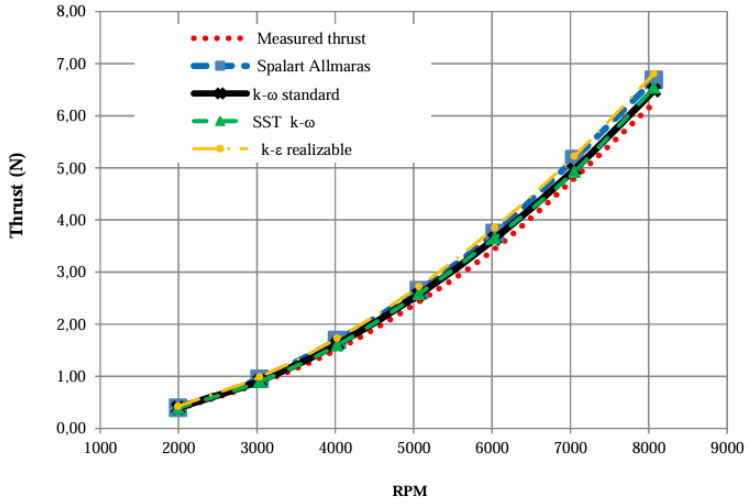

Source: From author.

As shown in Fig. 13, the thrust generated by the propeller as a function of rotation velocities, simulated using the SST K-ω turbulence model, agreed very well with the measured thrust for the entire propeller operating range. Observing Figure 14, it can be concluded that the simulation results for the power coefficients were much lower than the values measured at rotation speeds lower than 5,000 rpm. Between 5,000 and 8,000 rpm the results were very close, except for the k-ε realizable model. The average difference in power coefficients for the SST k-ω model, in comparison to the measured values, was 5.1% and the maximum difference was 15.9% at 2,000 RPM. As shown in Figure 15, all models agreed very well with the measured torque values except the realizable k-ε model.

Figure 14

Comparison between power coefficients with torque measured on the test bench and simulated by CFD with different turbulence models

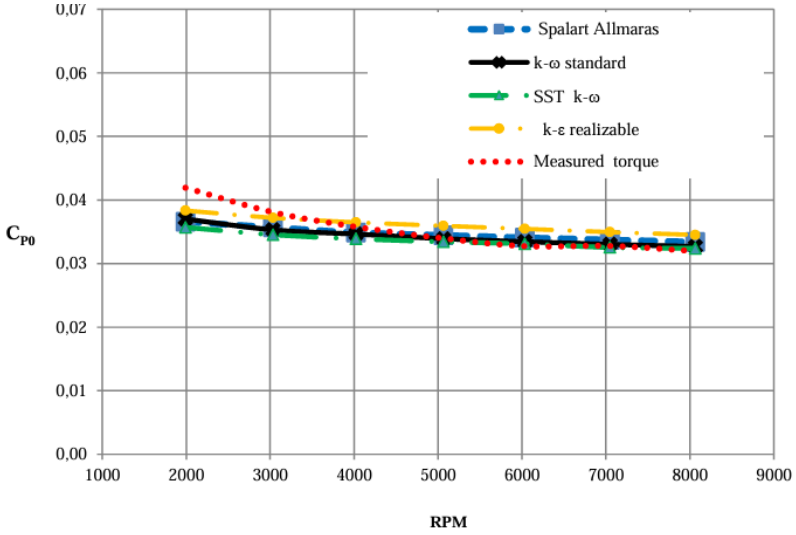

Source: From author.

Figure 15

Comparison between torque measured on the test bench and simulated by CFD with different turbulence models

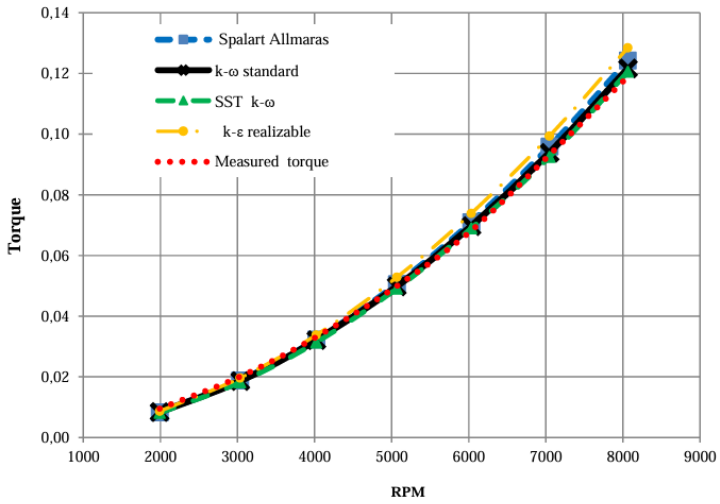

Source: From author.

It is important to highlight that the standard k-ω model had a very similar result to the SST k-ω model, both for the thrust coefficient and for the Power coefficient, as concluded by Seeni, 2021.

To verify whether the laminar-turbulent transition models obtain greater accuracy at low rotation rates, especially with regard to power coefficient, which showed a greater difference in relation to the measured values, simulations were performed with two models. Figure 16 presents the results of the power coefficient and the percentage difference of these

values calculated by the SST k-ω model and the γ model in relation to the measurements. An improvement in the results for low rotations rates can be observed, especially for the Intermittency Transition model (γ model), but the Transition SST model also presented better results than the fully turbulent models for low rotations rates. For speeds above 4,000 rpm, there was no significant difference between the transition models and the fully turbulent models. Figure 7 shows that above 4000 rpm, at the position r/R=0.75 (which corresponds to the Reynolds number calculated at the rotational rate at the 75% station), the Reynolds number is greater than 63,300. In conclusion, the study indicates that, for the propeller under analysis, with a Reynolds number equal to or less than 63,300 (4,000 rpm), fully turbulent models begin to show greater inaccuracy.

Comparing the results of the best laminar-turbulent transition model (γ model) with the best fully turbulent model (SST k-ω), in relation to the measurement, there was a drop in the average difference from 5.1% to 2.6% and for the 2,000 rpm rotation from 15.9% to 3.3%. It can be seen that below 5,000 rpm the transition model is much more accurate, however, from 5,000 rpm to higher velocities, the fully turbulent model becomes more accurate. It is also observed that for the laminar model, at rotations of 2,000 and 3,000 rpm, the results were very close to those of the γ model, with a difference of 1.1% and 0.5% for 2,000 and 3,000 rpm, respectively.

Figure 16

Comparison between power coefficients with torque measured on the test bench and simulated by CFD with transition turbulence models and the SST k-ω fully turbulent model

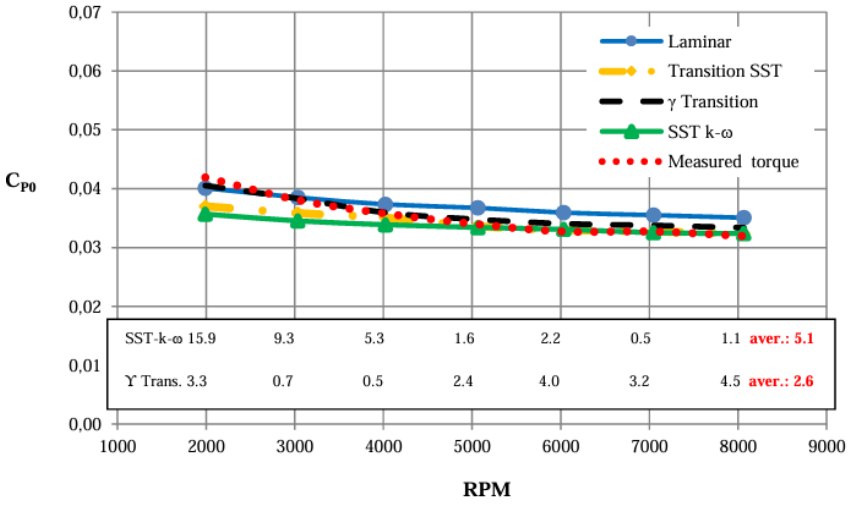

Source: From author.

As shown in Figures 13 and 15, at low rotation velocities there is a drop in the thrust coefficient and an increase in the power coefficient. As described by Deters, 2014, the change in thrust and torque coefficient, with the former decreasing and the latter increasing, is due to the reduction of the Reynolds number to below 100,000. At these values, a laminar flow separates from the propeller due to an adverse pressure gradient that imposes a region of recirculating flow, causing a reduction in lift and an increase in airfoil drag. Figures 16(a) and 16(b) show the visualization of the airflow separation around the propeller sections (airfoils) at r = 50.8 mm (r/R = 0.40) for rotations velocities of 2,000 rpm and 5,000 rpm. In the propeller section at r/R = 0.40, which has a Reynolds number of 18,000 at 2,000 rpm, the laminar separation bubble size is larger than in the same section at 5,000 rpm, with a Reynolds number of 44,900, because the bubble grows as the Re number decreases. Figures 16(c) to 16(f) show the airflow around the section at r/R = 0.75 (r = 95.3 mm) at rotation velocities from 2,000 rpm to 5,000 rpm. The flow separation length decreases with increasing speed. At 2,000 rpm, the flow separation length occupies about 75% of the airfoil and gradually decreases until it disappears at 5,000 rpm. These images were made with simulation data with the γ transition model. This observation is in agreement with the conclusions drawn in Figure 17, that is, from 5,000 rpm onwards, as flow separation is no longer observed, the fully turbulent model becomes accurate. Fully turbulent models have a critical limitation when applied to low Reynolds number flows: because they assume turbulence from the leading edge of the airfoil, they ignore transition effects and, therefore, they do not capture satisfactory the laminar separation bubble (LSB), resulting in an underprediction of the drag caused by the LSB. On the other hand, since laminar-turbulent transition models are able to capture LSBs, they can also capture the increased drag caused by them and, consequently, the increased power coefficient on the propellers.

Figure 17

Laminar boundary layer separation in propeller section

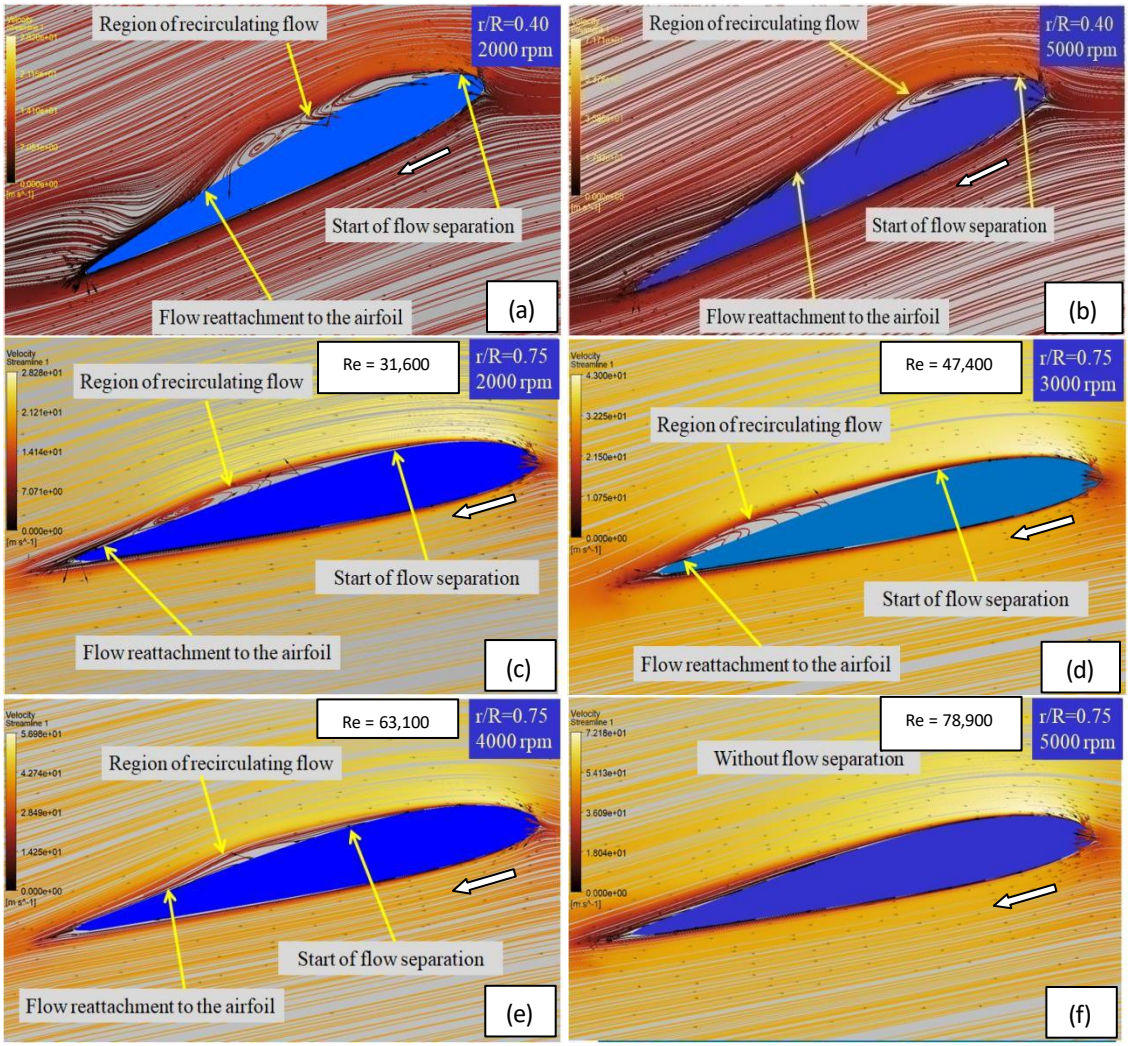

8 CONCLUSIONS

Considering turbulence models for low Reynolds number flows, the most suitable ones are those that capture the laminar-turbulent transition conditions, but they have the disadvantage of being computationally very intensive. Thus, for the small-scale propeller designed, operating in static performance, we seek to identify from which condition it is really necessary to use such models. The following conclusions were reached:

Full turbulence models can predict thrust and power coefficients for Reynolds numbers greater than 60,000. For values less than 60,000, they fail to predict, as they are not able to capture satisfactory effects of laminar boundary layer; Laminar-turbulent transition models should be used for Reynolds numbers less than 60,000, as they can capture laminar boundary layer effects and consequently the change in propeller power coefficients; The best models for Reynolds numbers greater than 60,000 are the SST k-ω and the Standard k-ω, since the accuracy compared to the transition models was very similar, in fact, being better

than the transition models for this range; The best model for Reynolds number less than 60,000 is the Transition γ model (Intermittency Transition model); Visual analysis through CFD of the flow around the propeller was consistent with the results related to the power coefficient, that is, through both analysis methods it was concluded that below 5000 rpm the transition models are more accurate and that for higher rotations from 5000 rpm the fully turbulence models are more accurate.

An important contribution of this work is the visualization through CFD of the characteristics of the laminar separation bubble, such as the beginning of the flow separation, the recirculation flow region and its reattachment to the propeller downstream.

REFERENCES

Ananda, G. K., Deters, R. W., & Selig, M. S. (2013). Propeller induced flow effects on wings at low Reynolds numbers. In 31st AIAA Applied Aerodynamics Conference.

Ansys. (2025). ANSYS Fluent Theory Guide. Canonsburg, PA, USA.

Cerny, M., & Breitsamter, C. (2020). Investigation of small-scale propellers under non-axial inflow conditions. Aerospace Science and Technology, 106, 106048.

Deters, R. W., Ananda, G. K., & Selig, M. S. (2014). Reynolds number effects on the performance of small-scale propellers. In 32nd AIAA Applied Aerodynamics Conference.

Divazi, A., Askari, R., & Roohi, E. (2025). Experimental and numerical investigation on the spraying performance of an agricultural unmanned aerial vehicle. Aerospace Science and Technology, 160, 110083.

Dougherty, S., Oo, L. N., & Zhao, D. (2024). Effects of propeller separation and onset flow condition on the performance of quadcopter propellers. Aerospace Science and Technology, 145, 108837.

Drela, M. (2006). QPROP formulation. MIT Aero & Astro.

Garofano-Soldado, A., Sanchez-Cuevas, P. J., & Heredia, G. (2022). Numerical-experimental evaluation and modelling of aerodynamic ground effect for small-scale tilted propellers at low Reynolds numbers. Aerospace Science and Technology, 126, 107625.

Kumar, R., Kumar, G., Zunaid, M., & Ansari, N. A. (2021). Numerical analysis of a quadcopter in different weather conditions of region in India. Materials Today: Proceedings, 43, 378–382.

Liu, Y., Kan, Z., Li, H., Gao, Y., Li, D., & Zhao, S. (2024). Analysis and modeling of the aerodynamic ceiling effect on small-scale propellers with tilted angles. Aerospace Science and Technology, 147, 109038.

Liu, X., Zhao, D., & Oo, L. N. (2023). Comparison studies on aerodynamic performances of a rotating propeller for small-size UAVs. Aerospace Science and Technology, 133, 10148.

Loureiro, E. V., Oliveira, N. L., Hallak, P. H., Bastos, F. S., Rocha, L. M., Delmonte, R. G. P., & Lemonge, A. C. C. (2021). Evaluation of low fidelity and CFD methods for the aerodynamic performance of a small propeller. Aerospace Science and Technology, 108, 106402.

Paz, C., Suárez, E., Gil, C., & Vence, J. (2021). Assessment of the methodology for the CFD simulation of the flight of a quadcopter UAV. Journal of Wind Engineering & Industrial Aerodynamics, 218, 104776.

Rajendran, P., & Jayaprakash, A. (2023). Numerical performance analysis of a twin blade drone rotor propeller. Materials Today: Proceedings, 80, 492–498.

Seeni, A. (2021). Effect of turbulence models in performance characterization of a low Reynolds number UAV propeller. INCAS Bulletin, 13, 151–166.

Weerasinghe, S. R., & Monasor, M. (2012). Simulation and experimental analysis of hovering and flight of a quadcopter. In 13th International Conference on Heat Transfer, Fluid Mechanics and Thermodynamics.

Zarri, A., Dell'Erba, E., Munters, W., & Schram, C. (2022). Aeroacoustic installation effects in multi-rotorcraft: Numerical investigations of a small-size drone model. Aerospace Science and Technology, 128, 107762.